

# DESIGN AND PERFORMANCE OF THE TERRESTRIAL PLANET FINDER CORONAGRAPH

Mary White<sup>1a</sup>, Stuart Shaklan<sup>a</sup>, P. Douglas Lisman<sup>a</sup>, Timothy Ho<sup>a</sup>, Pantazis Mouroulis<sup>a</sup>, Scott Basinger<sup>a</sup>, Bill Ledeboer<sup>a</sup>, Eug Kwack<sup>a</sup>, Andy Kissil<sup>a</sup>, Gary Mosier<sup>b</sup>, Alice Liu<sup>b</sup>, Chuck Bowers<sup>b</sup>, Carl Blaurock<sup>b</sup>, Terry Cafferty<sup>c</sup>,  
<sup>a</sup>California Institute of Technology, Jet Propulsion Laboratory, 4800 Oak Grove Dr., Pasadena, CA, USA, 91109;

## ABSTRACT

Terrestrial Planet Finder Coronagraph, one of two potential architectures, is described. The telescope is designed to make a visible wavelength survey of the habitable zones of at least thirty stars in search of earth-like planets. The preliminary system requirements, optical parameters, mechanical and thermal design, operations scenario and predicted performance is presented. The 6-meter aperture telescope has a monolithic primary mirror, which along with the secondary tower, are being designed to meet the stringent optical tolerances of the planet-finding mission. Performance predictions include dynamic and thermal finite element analysis of the telescope optics and structure, which are used to make predictions of the optical performance of the system

## 1. INTRODUCTION

Two different instrument architectures are being studied for the Terrestrial Planet Finder: a coronagraph and an interferometer. For both architectures, the design teams were chartered to develop two designs, one that will meet the full mission science goals and one that will meet minimum mission science goals. For all cases, the mission will include both discovery and characterization of planets. For discovery, the instrument is required to search for earth-like planets within the habitable zone of target stars. Characterization involves determination of the orbit and spectroscopic characteristics of the planet and its atmosphere. The TPF Coronagraph designed to meet the minimum mission goals is presented, along with analysis and performance predictions. Details of the TPF mission, modeling tools and error analysis are described in detail in companion papers ([1], [2], [3], [4], [5]).

## 2. REQUIREMENTS AND DESIGN OVERVIEW

### 2.1. Introduction

Briefly stated, the minimum mission goals are to survey 35 stars, searching the full habitable zone of each star to 95 percent completeness and characterize planets in the visible wavelength range. The full mission goals are survey 260 stars with an average completeness of 95 percent and to characterize any found planets.

The approach was to start with the requirements for the star survey, then to determine the required inner working angle and contrast for the system, develop an error budget (in units of contrast) for specific perturbations to the optical system. After the system was designed, integrated modeling tools were used to determine whether the requirements are met under flight conditions.

The initial design concept was the Ball Architecture Study done in 2002, which was responsive to a desire to search for more stars (about the same as is currently referred to as the Full Mission). The result of the Ball Architecture Study was a coronagraph system with a 10 x 4 meter primary mirror ([6]). In designing a system for the Minimum Mission the architect and design team selected a 6 x 3.5 meter primary mirror. For the Minimum Mission, there was a strong preference for making conservative design choices, i.e., conventional materials, passive thermal design and a launch vehicle for which NASA has a contract in place. The primary challenge was to design an optical system and provide a

---

<sup>1</sup> [marie.levine@jpl.nasa.gov](mailto:marie.levine@jpl.nasa.gov); phone 1-818-354-9196

thermally and structurally stable environment for that optical system that will meet the requirements stated for the Minimum Mission. The actual performance of that system would be determined at the completion of the analysis task, a few months later.

## 2.2. Optical Layout

The optical design of the minimum mission has been adapted to accommodate classical as well as shaped-pupil coronagraph concepts. The telescope is a Cassegrain-like design with an elliptical aperture of 6x3.5 m. The secondary mirror is located approximately 10 m away, and has an aperture of 0.7x0.44 m. The combination produces a F/20 beam (F-numbers considered along the major axis). A field stop can be located at the primary focus. Two fold mirrors direct the beam behind the primary mirror to the instrument box. The fold mirrors are crossed to minimize polarization dependence. A ray trace of the entire system is shown in [Figure xxxx](#).

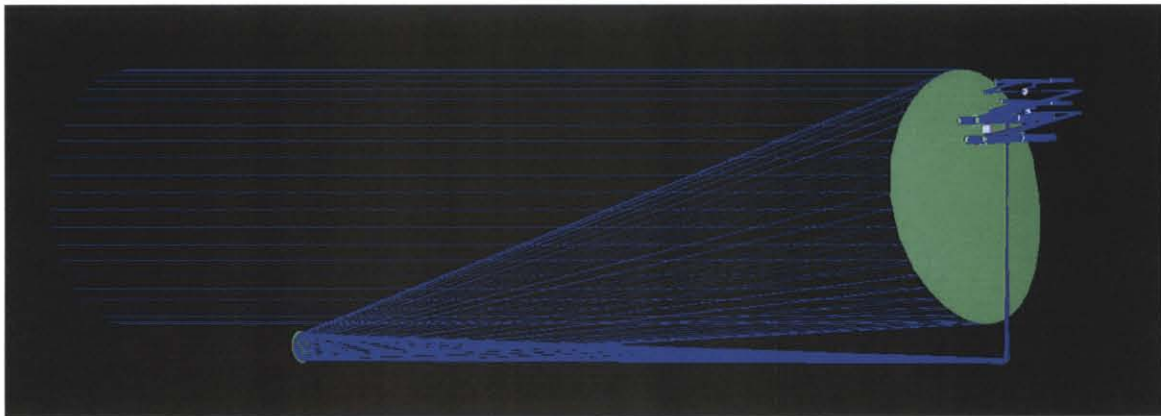


**Figure xxxx.** Raytrace of the full optical system.

An off-axis parabolic collimator provides a collimated beam of 10 cm major axis where the polarizers and deformable mirrors are located. A polarizer assembly is comprised of three beamsplitter “cubes”, the first of which acts as a polarizing beamsplitter to separate x and y polarizations, while the other two are inserted in each beam to improve the extinction.

Two deformable mirrors follow, arranged as the mirrors of a Michelson interferometer (one for the x and one for the y polarization) provide amplitude and phase compensation. The Michelson interferometer uses a beamsplitting “cube”, followed by a tilted compensating wedge. This arrangement gives negligible angular dispersion, hence practically zero chromatic error at the focal plane. It also gives very small linear dispersion, so that blue and red rays are not only parallel as they reach the DM but also essentially coincident. The polarizer and Michelson assembly is shown in [Figure xxxx](#).

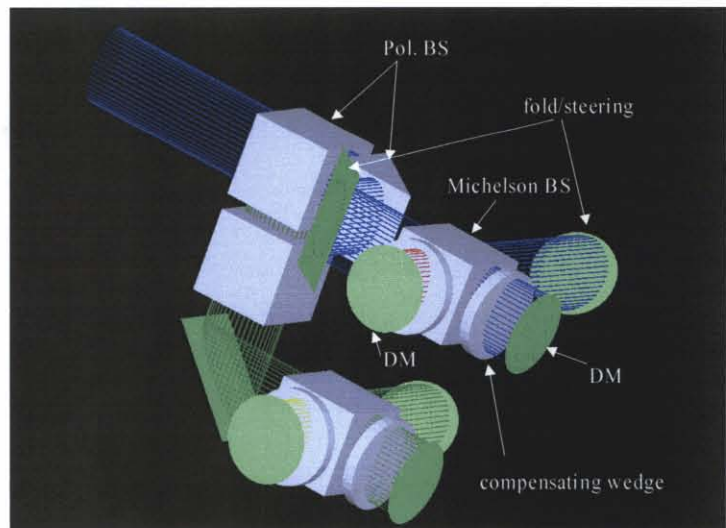


**Figure xxxx.** Polarizer and Michelson assembly.

Two fold mirrors, one between the polarizing beamsplitter and the Michelson assembly, and the second at the exit of the Michelson serve as steering mirrors. A two-parabola afocal relay is used to reimagine the pupil from the deformable mirror location to a plane where a shaped pupil mask can be employed. The relay is followed by a 6 m focal length mirror, which focuses the beam at F/60 to the occulting mask. A small fold mirror is necessary before the occulting mask in order to package the optical system in the box. The theoretical wavefront performance of the entire telescope assembly up to this point is  $3e-4$  waves p-v, with no chromatic error.

A collimating mirror after the occulter provides a location for the Lyot stop in a collimated space. The size of the beam at this point is 50 mm (major axis). A focusing mirror gives an F/20 beam at the image plane. A 1:1 three-mirror image relay is may be implemented at the end to provide additional flexibility in accommodating additional design requirements. The theoretical wavefront error at the center of the field is 0.12 waves p-v.

A 3-D raytrace model of the arrangement is shown in [Figure xxxx](#), starting at the second fold after the secondary mirror.

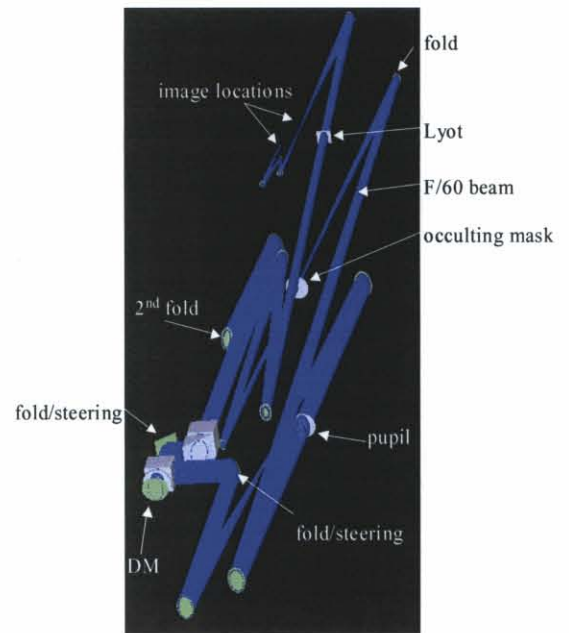


**Figure xxxx. Optical path (one) following the polarizing beamsplitter.**

### 2.3. Error Budget

The goal of the TPF coronagraph is to reduce diffraction and scattered light near the image of a star to the levels consistent with the light of a terrestrial planet orbiting the star in its habitable zone (where liquid water exists). The residual light level relative to the stellar light (if the coronagraph was not used) is called ‘contrast.’ The TPF contrast goal is  $1e-10$ . For detection of a planet, the contrast must be stable to a level of  $1e-11$  for several hours.

The TPF coronagraph error budget comprises the static and dynamic terms that contribute to image plane contrast. Static terms include wave front sensing and control, stray light, coronagraph mask leakage, and polarization leakage. Dynamic terms include any contribution to wave front error caused by motion of an optic or bending of an optic due to vibrations or thermal effects. Motion of optics induces aberrations and lateral beam walk, both of which scatter light where a planet might be found. Aberrations arise as the system is perturbed from its ideal design. Beam walk is the result of motion across non-ideal (real) optics. The former term is design-dependent, the latter, referred to as ‘beam walk,’ depends on the manufactured quality of the optics. Beam walk does not play a role if the optics are perfect.

[Figure xxxx](#) shows the error budget tree for an image evaluated at an angle of  $3 \lambda/D$ , where  $\lambda$  is the wavelength of the light and  $D$  is the telescope diameter. The minimum mission TPF design is required to work at  $3 \lambda/D$  (and larger angles) to provide adequate angular resolution. The numerical values in the figure are contrast. Since contrast is proportional to energy in the image plane, all contrast terms add linearly. Thus, the terms in the contrast error budget are simply summed; they do not add as the root-sum-square.

### TPF Coronagraph Error Tree: $3\lambda/D$

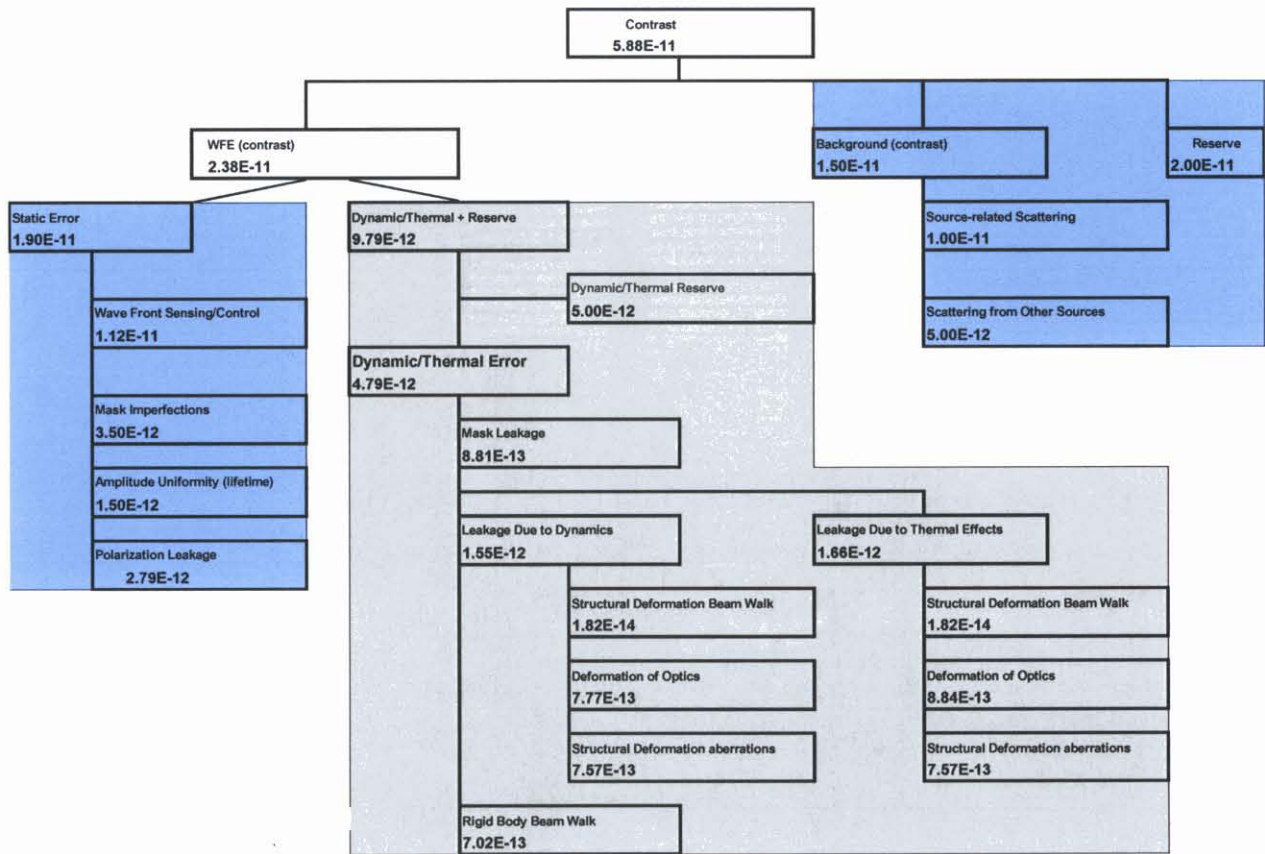


Figure xxxx. Error budget tree.

### 3. Mechanical Design

A schematic, Figure xxxx, shows the basic concept behind the mechanical configuration that incorporates the thermal design and illustrates the single structural load path between the telescope system and spacecraft. The schematic shows that the primary mirror, optical bench/coronagraph sensor instrument and thermal enclosure and secondary mirror structure are all independently supported on an aft metering structure (AMS). The AMS is then mounted on a vibration isolation system that is connected to the spacecraft. This key structural feature of the design isolates the telescope and sensor system from the spacecraft so that transmissions of jitter and reaction wheel disturbances are minimized.

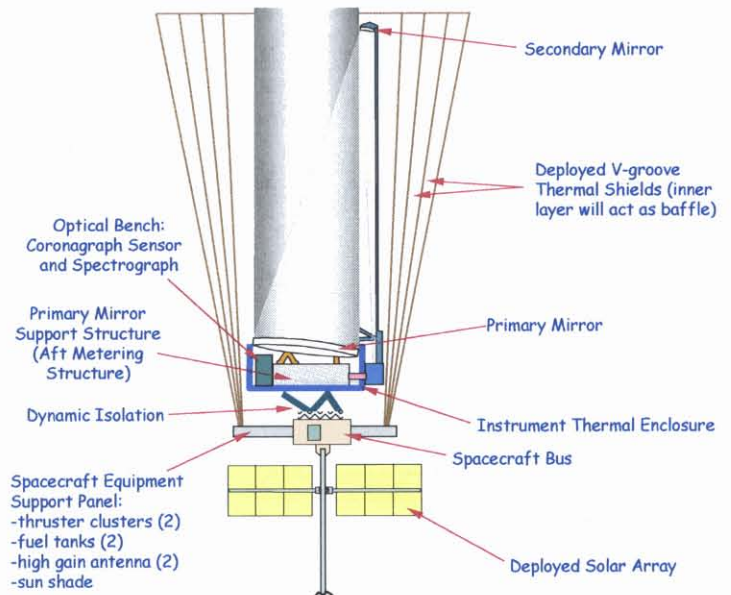
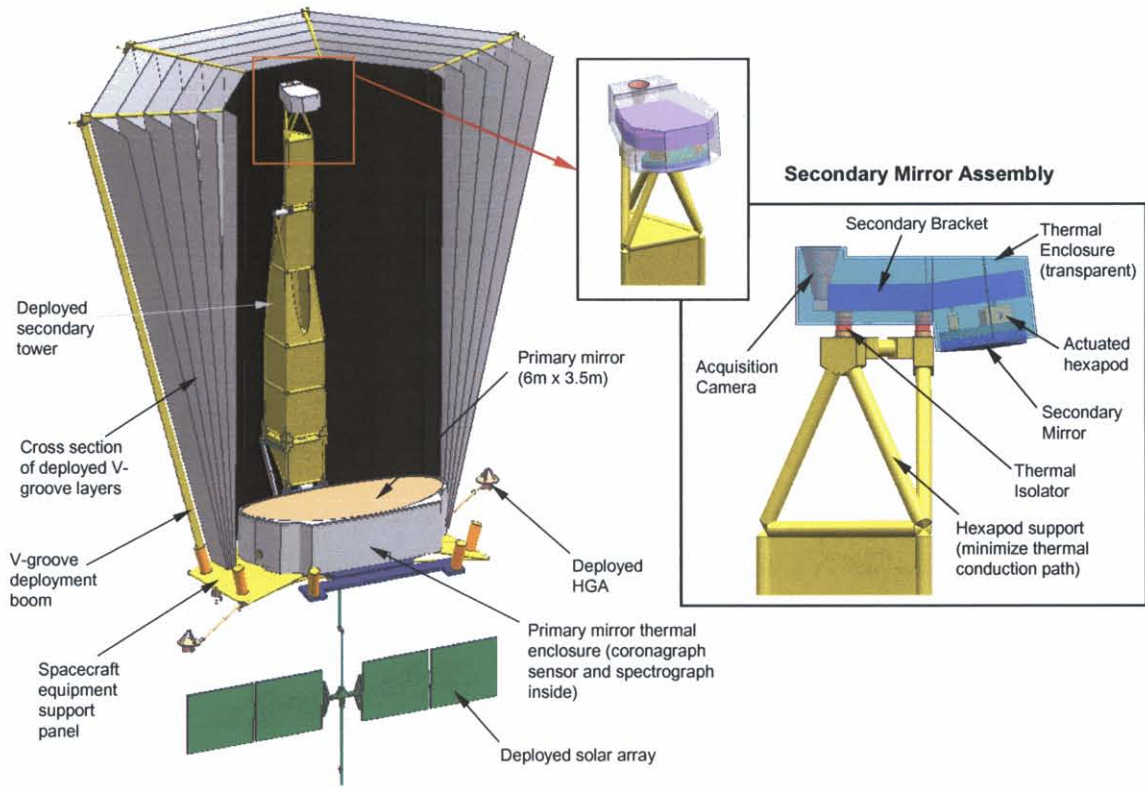


Figure xxxx. Configuration schematic.

A closer look at the telescope system with a cut away of the thermal v-groove shield is shown in **Figure xxxx**. The telescope system consists of a 6 m by 3.5 m ellipsoid primary mirror and a secondary mirror spaced 10 m away from the primary. The secondary mirror is supported on a deployable tower that stows for launch. The secondary mirror is supported at the tip of the tower on a hexapod structure that is thermally isolated from the secondary bracket. A thermal enclosure surrounds the components of the secondary mirror. An actuated hexapod is mounted to the backside of the secondary mirror for coarse alignment of the secondary to primary mirror.



**Figure xxxx. Telescope and Secondary Mirror assembly.**

**Figure xxxx** shows the layout of the components behind the primary mirror. Clearly, the AMS is the main support structure for the primary mirror, secondary tower, optical bench, and thermal enclosure while also providing the major tie-down locations to the launch vehicle. The primary mirror is supported to the AMS with 3 bipods that will need to be locked for launch. The thermal enclosure and optical bench are also attached to the AMS with 3 bipods. The location of the optical bench is

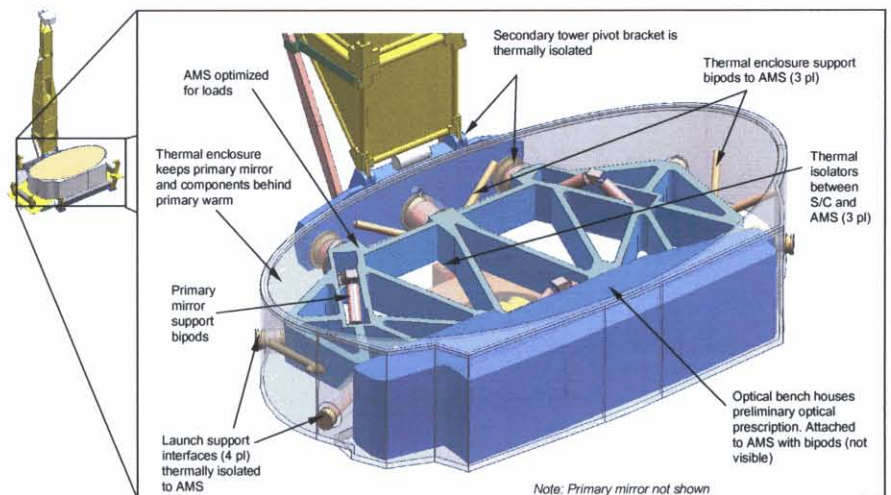


**Figure xxxx. Aft Metering Structure.**

advantageous because it can be assembled and tested off the AMS and then integrated on.

The underside of the AMS is attached to the spacecraft bus with thermal isolators that are attached to the vibration isolation system. As mentioned earlier, this is the only connection between the AMS and the spacecraft components.

There are four struts that protrude from the thermal enclosure that are interfaces to the launch shroud. The interfaces support the telescope in the launch shroud.

Several major spacecraft components have been defined and placed in the configuration. Most everything is attached to the spacecraft equipment panel. The platform has a truss structure backing that attaches to the spacecraft. At this time the design includes the reaction wheels placed in the center of the spacecraft bus and as close to the system C.G. as possible, two propellant tanks, two thruster clusters, the high gain antennas on deployable beams that will position the antennas so that they have a view beyond the v-groove sun shade, solar arrays.

The solar sail is designed to be 4.8 m x 14 m in size. It is deployed by a canister boom and positioned at the end of a deployable arm off the solar array arm.

To stow the vehicle, the secondary tower folds down, the v-groove platform folds under the spacecraft equipment panel, the high gain antenna arms fold along side the ends of the spacecraft equipment panel and the solar arrays and sail fold up behind the spacecraft. The stowed configuration is supported in the launch shroud with a bipod arrangement at the structural locations on the AMS and corners of the spacecraft equipment truss to a cylindrical launch support structure. The cylindrical support structure attaches to the payload adapter fitting of the booster vehicle. The cylindrical support structure is closed on the ends to help minimize contamination on the primary and secondary mirror surfaces.

Once separated from the booster, the cylindrical launch support structure will separate from the flight system in a clamshell fashion. Motor actuators will deploy the v-groove platforms and secondary tower, and spring loaded hinges will deploy the high gain antennas, solar array and position the solar sail. A deployable mast will extend the solar sail.

#### **4. Thermal Design**

The extremely small allowance for thermal/dynamic disturbance of the coronagraph optics during its long-integration observation sequences requires that the thermal design of the system provide a very high degree of isolation from both external and internal disturbances. The thermal design for the minimum mission has been based on either an L2 halo orbit, or an Earth drift-away orbit, which are thermally equivalent. In these orbits, the only significant external thermal disturbance is the Sun. The observatory must be capable of observing targets anywhere in nearly  $2\pi$  sr defined by its anti-solar hemispherical field of view. And since observational strategies require various rolls, dithers and slews, each one more or less moving the solar vector, the thermal control system must effectively deal with the solar-induced transient thermal loading on the observatory. Our fundamental approach is to (through effective shielding) decouple the optics from the Sun effectively enough that the time scale associated with the buildup of solar induced distortion is sufficient to allow observation to be completed before thermal distortion becomes excessive.

To provide isolation from the Sun, the system includes a quasi-conical multi-staged 'cocoon' v-groove shield wrapped around the length of the telescope, as shown in [Figure xxxx](#). Early analytical results are promising.

#### **Figure xxxx. Cocoon Concept Schematic**

A 'hybrid' thermal control approach was chosen for initial evaluation. In this hybrid approach, the primary mirror and the optical bench, aft metering structure (AMS) and coronagraphic sensor behind it are surrounded by a highly thermally conductive, actively controlled 'isothermal enclosure'. This enclosure is de-coupled from the Sun and spacecraft by means of conventional thermal isolation, and controlled in all zones to the highest possible precision, at a temperature level above its equilibrium temperature under the influence of external sources. This isothermal enclosure

is radiatively coupled strongly into the optics bench, AMS, coronagraph instrument and primary mirror backside, in a manner such that the primary mirror is maintained near the temperature at which it was tested on the ground.

The reflective side of the primary mirror is coupled to cold space and the interior surface of the black stray light baffle that is the innermost surface of the v-groove shield set. Since the baffle is extremely well isolated from the Sun by the v-groove stack, and since it also sees cold space, it gets cold and radiatively draws energy out of the face of the primary mirror, which in turn draws energy out of the structure behind it.

A similar approach is taken in stabilizing the secondary mirror assembly, which also must operate near 'room' temperature. That is, another 'isothermal enclosure' surrounds its backside, its critical active alignment features, and the fine guidance sensor head.

The M1-M2 metering structure is thermally isolated from the primary and secondary support structures, covered with thermal blankets and allowed to achieve thermal equilibrium inside the baffle. The outer layer of the secondary tower MLI blankets is blackened for stray light control purposes.

The design approach postulates that the achievable precision of active thermal control on the isothermal cavities is such that, when the control instabilities (presumed to be at the ~10mK level) are damped through the RC radiative coupling into the relatively large thermal mass of the critical optics assemblies, the resulting instability of the alignment-critical elements will be within acceptable limits. And the carbon fiber reinforced plastic (CFRP) M1-M2 metering structure, since it is housed within thermal blankets inside the relatively stable baffle, is expected to remain thermally and dimensionally stable within transient limits consistent with the observation scenario.

#### **4.1. V-groove Shield System Deployment**

In order to fit a large V-groove sunshade into any launch vehicle shroud it needs to be deployed in space. In the minimum mission design, the deployment takes place in steps. First, the back end structure supporting deployment booms unfolds. Next, the booms extend to pull the fabric of the V-groove layers upwards, roughly parallel to the telescope optical axis. The final step will be to tension the fabric and pull it outward radially so that the layers separate and form the v-groove geometry that enables this concept to function.

#### **4.2. Materials and Coatings**

The v-groove radiator consists of 6 layers of shielding of ~0.05 mm thick Kapton. Each side of the Kapton is coated with ~ 1000 angstroms of vapor-deposited aluminum (VDA) to reduce radiant coupling between shield layers. This material is highly specular at the relatively long IR wavelengths associated with the internal shield layers. The two exceptions to this are the inner and outermost surfaces. The inner surface is optically black in order to provide stray light control around the primary and secondary mirrors. The outer surface is second surface mirror silvered Teflon (TBR) to provide maximum solar heat load rejection while retaining high IR emittance.

### **5. Pointing Control System Design**

The Pointing Control System (PCS) design for the TPF Coronagraph combines a three-axis, inertial-stabilized Attitude Control System, a fine guidance sensor and a two-axis fine steering mirror. The top-level requirements for the PCS/isolation system, derived from the contrast error budget and the science operational efficiency budget.

#### **5.1. Target Acquisition and Observation Scenario**

Nominal target acquisition and observation proceeds in three phases. Each subsequent phase has a distinct sensor and an improved level of pointing accuracy.

- (1) Slew and Initial Acquisition - In this phase, the system is slewed, using gyros, to a commanded inertial attitude. Stars are acquired by the star trackers, which are located in the spacecraft, in a coarse pointing mode.
- (2) Acquisition Camera - The acquisition camera will bridge the gap between the pointing accuracy of the star tracker system ( $\sim 7''$ ) and the limited coronagraphic field of view ( $r \sim 1''$ ) of the fine guidance sensor. The acquisition camera should have a field-of-view of at least  $r \sim 30''$  to provide good overlap with the star tracker system. The acquisition camera must detect the target in its FOV and provide a correction signal to the S/C to position the target within the  $\sim 1''$  FOV of the fine guidance system. At this point, pointing is no longer with respect to an inertial frame. The acquisition camera is located near the telescope prime focus using a pick-off mirror, which incorporates a hole for transmission of the coronagraphic FOV. In this case, the camera can be a visible CCD and is required to determine the location of the target star (centroid) and have knowledge of the location of the FOV of the coronagraphic system. After providing an error signal to the S/C, the target is within the FOV of the fine guidance camera and the acquisition camera is not used until the next target acquisition sequence.
- (3) Fine guidance system - The fine guidance system consists of a fine guidance camera (FGC) and fast steering mirror (FSM). The camera is designed to provide error signals to the steering mirror in order to achieve the 0.11 mas centroid motion (LOS) stability. The steering mirror tip/tilt motions are fed back to the ACS control system to reduce the boresight error from the value transferred by the acquisition camera ( $< 1''$ ) to the required level ( $< 0.8 \text{ mas}$ ). The camera is a CCD based system. The image of the coronagraph FOV is transmitted to the FGC by reflection off the back of the substrate holding the coronagraph obscuring spot. Detection of stellar position appears possible using centroiding. Error signals are transmitted to the FSM by the FGC for jitter correction. In addition the orientation of the FSM with respect to nominal alignment position is monitored (the position for perfect alignment on the boresight), and transmitted to the S/C to keep any drift of the boresight within the required limits.

## 6. Analysis Process

For the investigation of the minimum mission design it was determined that the simulation of the "dither" sequence would constitute a bounding condition for the coronagraph system performance assessment. A dither sequence is a  $20^\circ$  roll about the line of sight (LOS) during which the wavefront stability must be maintained within the requirements without recalibration from the deformable mirrors during a period of observation of approximately 2 hours ( $\sim 10000 \text{ sec}$ ). To search the full habitable zone with the telescope having an elliptical aperture, a second dither sequence at  $90^\circ$  from the preceding one is required. The system is allowed time to reach thermal equilibrium and the wavefront is reset between the first and second set of dithers.

The goal of the thermal stability analyses is to predict the wavefront (WF) distortions and contrast degradation due to thermal transient conditions. For now, the analysis considers the contributions from rigid body and figure distortions of the primary mirror (PM). The current design assumes an active or passive secondary mirror (SM) truss alignment capability with a bandwidth of  $\sim 1 \text{ Hz}$  which will mitigate any slow thermal drifts in the SM position. As the design and models mature, we will increase the fidelity of the models to include perturbation effects from all the components. Wavefront error (WFE) is computed using Modeling and Analysis for Controlled Optical Systems (MACOS) from the structural distortions through the use of the optical sensitivity ("C") matrix, which provides a linear relationship between structural displacements and WFE. Use of the C matrix allows quick and efficient investigations of mechanical and thermal design options. The relationship between WFE and contrast is quadratic (i.e., non-linear), so that an exact calculation in MACOS is required to assess the contrast performance to the various sources of WF perturbations.

The current scope of the jitter analysis is to investigate the pointing stability, the WFE and the contrast due to broadband RWA disturbances, the decay rate after a slew, and some preliminary trades on the vibration reduction strategies. Similarly to the thermal distortion analysis, an optical sensitivity C matrix is used to compute the WFE from vibration distortions, and contrast is computed directly with MACOS. For dynamic distortions the SM rigid body (RB) motions are included in the analysis since the SM passive/active control bandwidth ( $< 1 \text{ Hz}$ ) is below the RWA disturbance spectrum.

## 6.1. Opto-Mechanical Sensitivity Analysis

Rigid body perturbations were determined for each optic in the optical beam path. Since the primary mirror is much larger than any other optic, the effect of allowing the primary mirror to flex as prescribed by the mid-fidelity finite element mode was studied. The rigid body perturbations (x-rotation, y-rotation, z-rotation, x-translation, y-translation, and z-translation) are exercised in the global coordinate system. To compute the sensitivities of the primary mirror flexible modes, each of the nodes was pushed a small amount, one at a time, in the z-direction. A sensitivity matrix was computed for the wavefront error associated with allowing each node of the primary mirror to act as an “influence function.” The contrast for the calculated wavefronts can be computed from the error budget by decomposing the wavefronts into the first 15 Zernike terms and applying the individual contribution to the contrast from the coefficient of each Zernike term.

## 7. Performance Summary

### 7.1. Thermal Distortions of the Primary Mirror

The primary mirror must maintain its figure during a dither sequence. Since the sunshield is not circular symmetric the heat load on the system changes with roll angle. Two dither sequences would have the least amount of change of heat load to the system. Those are 80 to 100 degrees and 170 to 190 degrees.

- Of the two orthogonal 20 deg roll/dither maneuvers, 80 to 100 degrees and 170 to 190 degrees, the 80 to 100 degrees results in larger primary mirror low order Zernike aberrations.
- For the 80 to 100 deg roll/dither, the uniform CTE assumption produces non-conservative results, such that CTE variability must be considered to properly evaluate performance.
- The primary mirror response to the 80 to 100 deg roll/dither meets requirement specifications for 1.6 hours of transient response after the maneuver, with coma and trefoil being the worst aberration components, and does not meet requirement specs for the steady-state response.
- The primary mirror response to the 170 to 190 degree roll/dither meets requirement specifications for the thermal steady-state and transient responses.

### 7.2. Steady-state LOS Jitter and WFE for Benchmark Slew

The point design, with 0.75Hz first state isolation and 2Hz RWA isolation meets the LOS and WFE requirements. The Image Motion LOS requirements are met by passive isolation without relying on the FSM compensator. The worst-case LOS jitter due to RWA disturbances are shown in Table xxxx compared to the 3 lambda/D requirements. LOS jitter is substantially under the requirement. Table xxxx tabulates the rigid optics Zernike amplitudes (worst case over wheelspeed) compared to the requirements. All Zernikes meet requirements, with Zernike mode 9 the closest to its requirement. Table xxxx tabulates the Zernike amplitudes due to deformation of the optics. Zernike mode 8 shows a slight exceedance. However, this exceedance occurs at 3 Hz (the minimum allowed wheelspeed) and so can be accommodated by running the wheelspeed faster than 3Hz.

The benchmark steady-state results show that a properly designed system can meet the stringent performance requirements under RWA excitation. The benchmark results also help to create an understanding of the critical design issues. The analysis can now proceed to explore various design options (looking for a cost/risk optimal design) and simultaneously examine the effects of modeling uncertainty and non-idealities.

### 7.2.1. Slew/Settle Analysis Results for Transient Benchmark Slew

The current two-stage isolation and control designs do not meet all the slew/settle time requirements. Table xxxx summarizes the slew plus settle time observed in the simulation. Note that these are the first-cut analysis results, and many improvements can be made to reduce the settling time. Please see the future work section for more information.

**Table xxxx Slew/Settle Time Results**

	Slew+Settle Time (sec)	Time Requirement (sec)
LOS X	845	1200
LOS Y	1300	1200
Rigid Body Pitch ( $\theta_x$ )	1300	1200
Rigid Body Yaw ( $\theta_y$ )	1180	1200

### 7.2.2. General Assessment

The modeling results are encouraging. The design meets the stringent performance specifications in almost all areas, including ACS, dynamics, and thermal sensitivity. We have modeled the dynamic motion of the optics and find, not surprisingly, that it is dominated by motion of the primary and secondary mirrors, but these motions do not induce aberrations that exceed the requirements. We have modeled the thermal sensitivity of the primary mirror following rotations about the line-of-site and find that for some modes the deformation reaches a steady-state position that exceeds the allowed change.

The thermal result is conservative. We have treated each Zernike aberration as imposing a not-to-exceed requirement on bending of the mirror. However, a more relevant performance requirement is the summed Zernike contrast contribution. Using this result, the allowed post-dither integration time increases from 1.6 hour to ~ 3 hours.

We have not yet modeled the thermally induced motions of the secondary mirror. The requirements on motion of the secondary relative to the primary are very tight – the z (line-of-sight) motion requirement is 0.25 nm. We realize that it is unlikely that a secondary mirror tower composed of metal and composite materials (not to mention hinges), will ever achieve this level of stability. Therefore, our design includes a high-precision metrology truss, based on Space Interferometry Mission technology, to monitor the positioning of the secondary relative to the primary. The required precision, ~ 0.2 nm r.m.s. and 3e-11 relative frequency stability for several hours, exceeds SIM requirements but is technologically within reach. The metrology signals are used to drive a hexapod mounted to the back of the secondary mirror. The design of this hexapod is the subject of future studies.

Much work remains and this work represents only the first steps in modeling and design. Improvements can be expected in thermal stability as we identify the largest sources of thermal gradients and isolate them from the primary mirror. Dynamics margin will improve as we identify weak points in the structure. Both thermal and dynamic performance will improve as we optimize material selection. We will also revisit the error budget allocations so that they are better-matched to performance predictions. An important goal for future work is to increase model fidelity, as outlined below.

## 8. Summary

The modeling results are encouraging. The design meets the stringent performance specifications in almost all areas, including ACS, dynamics, and thermal sensitivity. We have modeled the dynamic motion of the optics and find, not surprisingly, that it is dominated by motion of the primary and secondary mirrors, but these motions do not induce aberrations that exceed the requirements. We have modeled the thermal sensitivity of the primary mirror following rotations about the line-of-site and find that for some modes the deformation reaches a steady-state position that exceeds the allowed change.

We have not yet modeled the thermally induced motions of the secondary mirror. The requirements on motion of the secondary relative to the primary are very tight – the z (line-of-sight) motion requirement is 0.25 nm. We realize that it is unlikely that a secondary mirror tower composed of metal and composite materials (not to mention hinges), will ever achieve this level of stability. Therefore, our design includes a high-precision metrology truss, based on Space Interferometry Mission technology, to monitor the positioning of the secondary relative to the primary. The required precision,  $\sim 0.2$  nm r.m.s. and  $3e-11$  relative frequency stability for several hours, exceeds SIM requirements but is technologically within reach. The metrology signals are used to drive a hexapod mounted to the back of the secondary mirror. The design of this hexapod is the subject of future studies.

Much work remains and this work represents only the first steps in modeling and design. Improvements can be expected in thermal stability as we identify the largest sources of thermal gradients and isolate them from the primary mirror. Dynamics margin will improve as we identify weak points in the structure. Both thermal and dynamic performance will improve as we optimize material selection. We will also revisit the error budget allocations so that they are better-matched to performance predictions. An important goal for future work is to increase model fidelity, as outlined below.

The thermal result is conservative. We have treated each Zernike aberration as imposing a not-to-exceed requirement on bending of the mirror. However, a more relevant performance requirement is the summed Zernike contrast contribution. Using this result, the allowed post-dither integration time increases from 1.6 hour to  $\sim 3$  hours.

1. D. R. Coulter, *NASA's Terrestrial Planet Finder Mission*, SPIE Astronomical Telescope and Instrumentation Conf., Glasgow Scotland, June 2004. Paper [5487-55]
2. S. C. Unwin, C. A. Beichman, *Terrestrial Planet Finder: Science and Technology Overview*, SPIE Astronomical Telescope and Instrumentation Conf., Glasgow Scotland, June 2004. Paper [5487-57]
3. V. G. Ford, *The Terrestrial Planet Finder Coronagraph: Technology and Mission Design Studies*, SPIE Astronomical Telescope and Instrumentation Conf., Glasgow Scotland, June 2004. Paper [5487-182]
4. M. Levine, *Integrated Modeling Approach for the Terrestrial Planet Finder Mission*, SPIE Astronomical Telescope and Instrumentation Conf., Glasgow Scotland, June 2004. Paper [5487-18]
5. R. P. Linfield, *Wavefront amplitude errors for a TPF coronagraph: their effects and possible correction*, SPIE Astronomical Telescope and Instrumentation Conf., Glasgow Scotland, June 2004. Paper [5487-179]
6. N. J. Kasdin, *An Optical/UV Space Coronagraph Concept for the Terrestrial Planet Finder*, COSPAR. Paper 02-A-00235, 2002.